Applied Physics Express **8**, 032401 (2015)
http://dx.doi.org/**10.7567/APEX.8.032401**

Optical antennas for tunable enhancement in tip-enhansed Raman spectroscopy imaging

Imad Maouli[1], Atsushi Taguchi[1], Yuika Saito[1], Satoshi Kawata[1,2], and Prabhat Verma[1,2*]

[1]*Department of Applied Physics, Osaka University, Suita, Osaka 565-0871, Japan*
[2]*Photonics Center, Osaka University, Suita, Osaka 565-0871, Japan*
E-mail: verma@ap.eng.osaka-u.ac.jp

Received January 7, 2015; accepted February 3, 2015; published online February 20, 2015

The use of optical antennas in tip-enhanced Raman spectroscopy (TERS) makes it a powerful optical analysis and imaging technique at the nanoscale. Optical antennas can work as nano-light sources in the visible region. The plasmonic resonance of an antenna depends on its length; thus, by varying the length, one can control the enhancement in TERS. In this study, we demonstrated a fabrication method based on focused ion beam milling to realize optical antennas with desired lengths. We then measured the resonances of these fabricated antennas and performed TERS imaging of carbon nanotubes to demonstrate the antenna length dependence on plasmonic resonance.

An optical antenna is a subwavelength device that efficiently couples the energy from a free propagating radiation to a confined region with a size comparable to that of the antenna. In particular, if a conically shaped antenna with a nanometric apex is illuminated resonantly, it can act as a nano-light source.[1–6] The resonance of an optical antenna, however, depends on the geometry and material. One can trace the first use of metallic nanoparticles as antennas in microscopy way back in 1928.[7]

Tip-enhanced Raman spectroscopy (TERS) utilizes a sharp metallic tip as an antenna,[1–8] which is positioned on the sample by either atomic force microscopy (AFM) or scanning tunneling microscopy (STM). In the case of AFM-based TERS, the antenna is usually obtained by coating a thin metal layer on a semiconducting AFM cantilever tip, and in the case of STM-based TERS, a solid metallic tip is used as the antenna. The tip in either case confines the light to a few nanometers and enhances the optical signal by several orders. In order to perform nanoimaging through TERS microscopy, the tip is raster-scanned on the sample by AFM or STM.

Here, we discuss the case of AFM-based TERS, where metal-coated semiconducting cantilever tips are used as optical antennas. Among many metal coating techniques, metal evaporation under high vacuum is the most successful and popular technique in AFM-based TERS.[5] Even then, the reproducibility of these antennas with desired plasmonic resonances is a critical issue, and researchers have paid great attention to improve the fabrication technique to achieve a higher reproducibility.[9,10] This is because the resonances of such antennas can be controlled by either the choice of metal or the shape and size of the metal grains deposited on the cantilever tip, which is challenging to control and reproduce.[11–14] The choice of metal controls the resonance in the broader region, while the resonance can be fine-tuned by proper control over the size and shape of the metal grains on the tip.[15] An innovative way to control the size of the metal on the evaporated tip is to utilize focused ion beam (FIB) milling, which is expected to provide a precise control of the size of the metal as well as a much higher reproducibility.[12] Here, we demonstrate a method of precisely controlling the size of the metal on optical antennas using FIB milling, as illustrated in Fig. 1.

Apart from the choice of metal and the size of the antenna, the refractive index of the base material of the tip also plays an important role in tuning the plasmon resonance.[16] For a stronger resonance in the visible region, a lower refractive index of the base material is better suited. For this reason, we first oxidized the tip to convert the base material from Si (reflective index = 4.4 at $\lambda = 488$ nm) to SiO_2 (reflective index = 1.5 at $\lambda = 488$ nm). We then milled out a ring shape on the tip at a desired distance from the apex, using FIB that was directed perpendicular to the tip axis around the tip surface, as illustrated in Fig. 1(a). This process removed silicon dioxide from the outer part of the tip in the milled region, leaving silicon dioxide only near the axis. In the present study, the ring shape was milled out at distances of 100, 200, and 300 nm from the apex for three different tips. The width of the ring of about 100 nm, which created a mushroom-shaped apex, as can be seen in Fig. 1(a), produced a discontinuity on the surface of the tip that separated the apex from the rest of the tip surface. The advantage of this shape is that when metal is evaporated from the bottom, the mushroom-shaped apex creates a shadow and the metal is not deposited in the milled area, as illustrated in Fig. 1(b). This separates the metal on the apex from the metal deposited on the rest of the cantilever. The width of the milled area, which is about 100 nm, is sufficiently large to guarantee no plasmonic interaction between the metal on the apex and the metal on the rest of the cantilever,[17] making it a true finite-size tip of desired length. The tip therefore behaves similarly to a finite-size metallic antenna, whose length is selected during FIB milling. FIB images of the milled tips can be seen in Fig. 2(a).

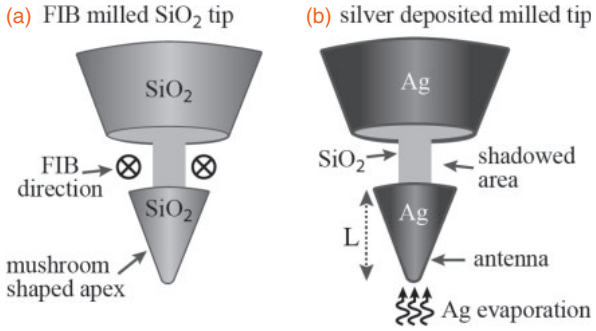

Fig. 1. (a) Illustration of FIB-milled ring shape on an AFM tip at distance L from the apex. (b) The mushroom-shaped apex can shadow the milled area during silver vapor deposition, and an antenna of length L, which is disconnected with the metal on the rest of the tip, can be formed at the tip apex.

We then thermally evaporated a silver layer on the milled AFM tips. The evaporator was set to evaporate a 60-nm-thick

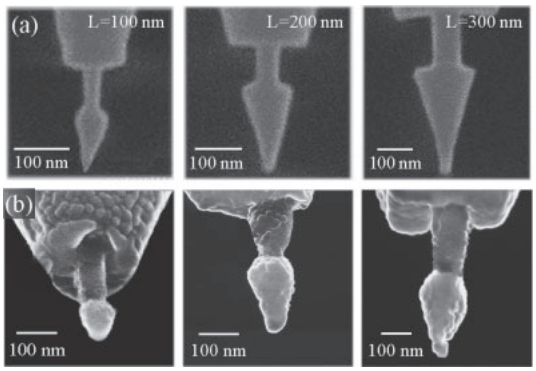

Fig. 2. (a) FIB images of FIB-milled AFM tips with different lengths, (b) SEM images of antennas with different lengths after the silver deposition.

silver layer at a rate of 1 Å/s under a high vacuum of 10^{-6} Pa. This thickness corresponds to a layer deposited perpendicular to the evaporation direction. However, in the case of sharply tapered tips, the actual deposited layer is much thinner. In the present case, the cone angle of the tip apex is 28°, and the thickness of the evaporated silver layer on the tip is about 15 nm. The radius of curvature at the tip apex before the evaporation is 5 nm, which, after evaporation, becomes 20 nm. We fabricated three antennas with lengths of 100, 200, and 300 nm, the SEM images of which are shown in Fig. 2(b). The fabrication method used has high precision and reproducibility, and it allows us to tune the plasmon resonance to a desired wavelength by selecting the size of the mushroom-shaped apex in the milled tips. From previous numerical and experimental studies,[12,13] we expect that a longer antenna will show a redshift in plasmon resonance.

In order to estimate the resonance wavelengths of the fabricated optical antennas, we applied dark-field scattering measurements. The dark-field microscope, illustrated in Fig. 3(a), was constructed using a xenon lamp that served as the incident white light source. The light was collimated and focused on a glass substrate via an objective lens (100×, NA = 1.49, oil immersion). A mask was introduced in the excitation path to cut the low-NA components so that the illumination light with only larger incident angles would approach the glass substrate and get totally internally reflected. The antenna, which was set on the other side of the glass substrate, was therefore illuminated by only an evanescent field. The antenna was positioned at the focus by an AFM feedback system. In order to avoid the strong background from the incident light, the scattered signal was collected only in the low- NA region by the same objective lens. The scattered light was introduced to a spectrometer and detected by a CCD camera. In order to remove any remaining background from the light source, the detected spectrum was normalized by the xenon lamp spectrum. The experimental results showed that the fabricated antennas with lengths of 100, 200, and 300 nm had resonances at 450, 510, and 590 nm, respectively. Figure 3(b) shows scattering spectra of the three fabricated optical antennas.

In order to confirm that the enhancement in TERS can be tuned with the length of the antenna, we performed TERS imaging of carbon nanotubes (CNTs) using our fabricated antennas. It is well known that CNTs show high Raman intensities when measured near the resonance condition. In

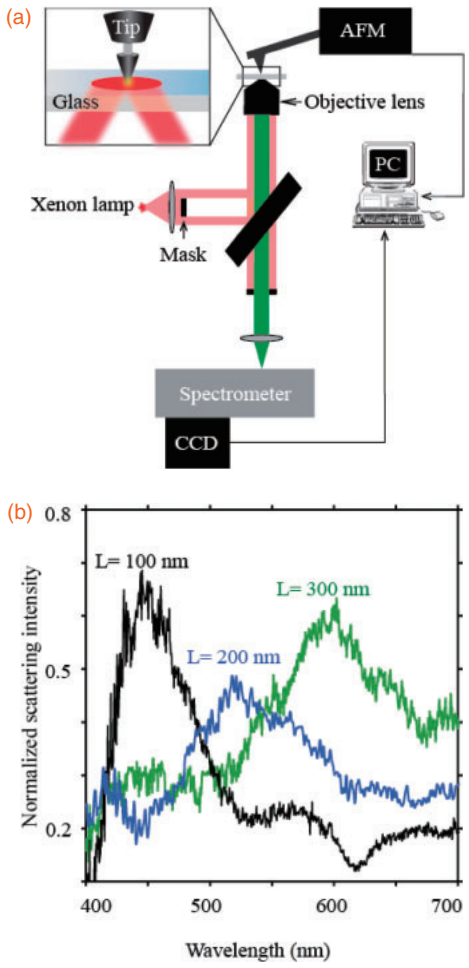

Fig. 3. (a) Schematic diagram of the experimental setup. (b) Scattering spectra of fabricated antennas with different lengths (L).

order to have a CNT sample that shows a near-resonance condition for a broad-wavelength region, we prepared our sample by mixing CNTs of several chiralities. These mixed CNTs were casted in the form of bundles on a glass substrate. The G-mode (1590 cm^{-1}) of our sample did not show any strong dependence on the incident wavelength used in the present work.[18] The CNT sample was illuminated with a p-polarized CW laser via an oil-immersion objective lens with NA equal to 1.49. The scattered signal was collected by the same objective lens, dispersed by a spectrometer, and recorded by a CCD camera. The antennas were positioned on the focus spot, and the CNT sample was scanned using the contact-mode feedback operation of the AFM system. We used three different illumination wavelengths, which were 473, 532, and 561 nm. The 473 nm illumination was in near-resonance with the antenna of 100 nm length, the 532 nm illumination was in near-resonance with antennas of 200 and 300 nm lengths, and the 561 nm illumination was in near-resonance with the antenna of 300 nm length. The results are presented by TERS images shown in Fig. 4, which were obtained for three different excitation wavelengths using the fabricated antennas of 100, 200, and 300 nm lengths.

Interestingly, TERS images show that we obtain higher enhancements for Figs. 4(a), 4(e), 4(f), and 4(i), where the incident wavelengths are in near-resonance with the antennas. The maximum enhancement factor of 1436 was estimated for

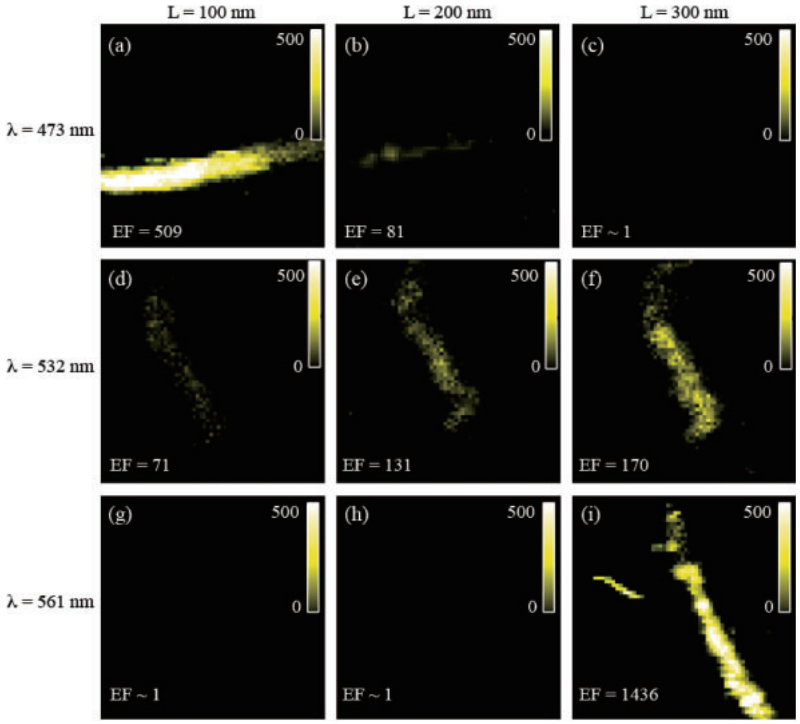

Fig. 4. TERS images ($320 \times 320\,nm^2$) of CNT samples, constructed from the G-band intensity. The exposure time for each pixel was 0.5 s. The abbreviations EF, L, and λ indicate the enhancement factor, the length of the antenna, and the illumination wavelength, respectively.

Fig. 4(i). The enhancement factor was estimated from the intensity ratio between the near-field and far-field measurements per unit area.[11] When the illumination wavelengths are far from the plasmonic resonances of the antennas, such as in Figs. 4(c), 4(g), and 4(h), TERS intensities are extremely low. This confirms that our fabricated antennas of different lengths can selectively show high enhancements for illumination near their plasmon resonance, which can be precisely controlled by choosing the length of the metal on the tip apex in our FIB fabricated tips.

Since nanosized samples have an extremely weak Raman scattering, it is advantageous to use an incident light with an energy close to the band energy of the sample for resonant Raman effects. This means that one would prefer to select a particular wavelength of the incident light for a given sample. Our fabrication technique comes very handy in such a case, because it can produce an antenna with the desired length that would selectively enhance a preferred incident wavelength. This precisely controlled tunability of Raman enhancement would be of tremendous advantage for samples with a weak Raman scattering.

In conclusion, we have demonstrated a fabrication method for optical antennas using FIB and thermal deposition of silver on AFM tips. We fabricated three antennas with different lengths of 100, 200, and 300 nm, and confirmed via scattering spectrum measurement that their plasmonic resonance wavelengths increased with increasing antenna length. The fabricated antennas were used for TERS imaging where we demonstrated that a high enhancement could be obtained when the illumination wavelengths were near the plasmonic resonance of a given antenna. Our technique can be used to fabricate antennas for TERS where one can very precisely control the antenna length and hence tune the plasmon resonance for better spectroscopic and imaging measurements. This would prove to be an important work where controlling a reproducible enhancement in TERS is still a challenge.

Acknowledgments The authors would like to acknowledge the financial support from the JSPS Asian Core Program and a Grant-in-Aid for Scientific Research (C) 24560028.

1) Y. Inouye and S. Kawata, Opt. Lett. **19**, 159 (1994).
2) Y. Inouye, P. Verma, T. Ichimura, and S. Kawata, in *Tip Enhancement*, ed. S. Kawata and V. M. Shalaev (Elsevier, Amsterdam, 2007) p. 90.
3) L. Novotny and B. Hecht, *Principles of Nano-optics* (Cambridge University Press, New York, 2006) 1st ed., p. 208.
4) P. Verma and Y. Saito, in *Nanoimaging with Optical antennas*, ed. M. Agio and A. Alu (Cambridge University Press, New York, 2012) p. 359.
5) S. Kawata, Y. Inouye, and P. Verma, Nat. Photonics **3**, 388 (2009).
6) L. Novotny and N. F. van Hulst, Nat. Photonics **5**, 83 (2011).
7) E. H. Synge, Philos. Mag. **6**, 356 (1928).
8) M. Sun, Z. Zhang, L. Chen, S. Sheng, and H. Xu, Adv. Opt. Mater. **2**, 74 (2014).
9) T. Umakoshi, T. Yano, Y. Saito, and P. Verma, Appl. Phys. Express **5**, 052001 (2012).
10) C. Blum, L. Opilik, J. M. Atkin, K. Braun, S. B. Kammer, V. Kravtsov, N. Kumar, S. Lemeshko, J. Li, K. Luszcz, T. Maleki, A. J. Meixner, S. Minne, M. B. Raschke, B. Ren, J. Rogalski, D. Roy, B. Stephanidis, X. Wang, D. Zhang, J. Zhong, and R. Zenobi, J. Raman Spectrosc. **45**, 22 (2014).
11) M. Fleischer, C. Stanciu, F. Stade, J. Stadler, K. Braun, A. Heeren, M. Häffner, D. P. Kern, and A. J. Meixner, Appl. Phys. Lett. **93**, 111114 (2008).
12) Y. Zou, P. Steinvurzel, T. Yang, and K. B. Crozier, Appl. Phys. Lett. **94**, 171107 (2009).
13) W. Zhang, X. Cui, and O. J. F. Martin, J. Raman Spectrosc. **40**, 1338 (2009).
14) W. Zhang, T. Schmid, B. Yeo, and R. Zenobi, J. Phys. Chem. C **112**, 2104 (2008).
15) H. Okamoto and K. Imura, J. Mater. Chem. **16**, 3920 (2006).
16) A. Taguchi, N. Hayazawa, Y. Saito, H. Ishitobi, A. Tarun, and S. Kawata, Opt. Express **17**, 6509 (2009).
17) S. Kawata, A. Ono, and P. Verma, Nat. Photonics **2**, 438 (2008).
18) X. Yan, T. Suzuki, Y. Kitahama, H. Sato, T. Itoh, and Y. Ozaki, Phys. Chem. Chem. Phys. **15**, 20618 (2013).